doi:10.1093/brain/awaa001 BRAIN 2020: 143; 684–700 | 684

BRAIN
A JOURNAL OF NEUROLOGY

Brain structural covariance networks in obsessive-compulsive disorder: a graph analysis from the ENIGMA Consortium

Je-Yeon Yun,[1,2] Premika S.W. Boedhoe,[3,4] Chris Vriend,[3,4] Neda Jahanshad,[5] Yoshinari Abe,[6] Stephanie H. Ameis,[7,8] Alan Anticevic,[9] Paul D. Arnold,[10,11] Marcelo C. Batistuzzo,[12] Francesco Benedetti,[13] Jan C. Beucke,[14] Irene Bollettini,[13] Anushree Bose,[15] Silvia Brem,[16] Anna Calvo,[17] Yuqi Cheng,[18] Kang Ik K. Cho,[19] Valentina Ciullo,[20] Sara Dallaspezia,[13] Damiaan Denys,[21,22] Jamie D. Feusner,[23] Jean-Paul Fouche,[24] Mònica Giménez,[25,26] Patricia Gruner,[9] Derrek P. Hibar,[5] Marcelo Q. Hoexter,[12] Hao Hu,[27] Chaim Huyser,[28,29] Keisuke Ikari,[30] Norbert Kathmann,[14] Christian Kaufmann,[14] Kathrin Koch,[31,32] Luisa Lazaro,[33,34,35,36] Christine Lochner,[37] Paulo Marques,[38] Rachel Marsh,[39,40] Ignacio Martínez-Zalacaín,[41,42] David Mataix-Cols,[43] José M. Menchón,[36,41,42] Luciano Minuzzi,[44] Pedro Morgado,[38,45,46] Pedro Moreira,[38,45,46] Takashi Nakamae,[6] Tomohiro Nakao,[47] Janardhanan C. Narayanaswamy,[15] Erika L. Nurmi,[23] Joseph O'Neill,[23,48] John Piacentini,[23,48] Fabrizio Piras,[20] Federica Piras,[20] Y.C. Janardhan Reddy,[15] Joao R. Sato,[49] H. Blair Simpson,[39,50] Noam Soreni,[51] Carles Soriano-Mas,[36,41,52] Gianfranco Spalletta,[20,53] Michael C. Stevens,[54,55] Philip R. Szeszko,[56,57] David F. Tolin,[54,58] Ganesan Venkatasubramanian,[15] Susanne Walitza,[16] Zhen Wang,[27,59] Guido A. van Wingen,[21] Jian Xu,[60] Xiufeng Xu,[60] Qing Zhao,[27] ENIGMA-OCD working group,* Paul M. Thompson,[5] Dan J. Stein,[24] Odile A. van den Heuvel[3,4] and Jun Soo Kwon[61,62]

*Appendix 1.

Brain structural covariance networks reflect covariation in morphology of different brain areas and are thought to reflect common trajectories in brain development and maturation. Large-scale investigation of structural covariance networks in obsessive-compulsive disorder (OCD) may provide clues to the pathophysiology of this neurodevelopmental disorder. Using T_1-weighted MRI scans acquired from 1616 individuals with OCD and 1463 healthy controls across 37 datasets participating in the ENIGMA-OCD Working Group, we calculated intra-individual brain structural covariance networks (using the bilaterally-averaged values of 33 cortical surface areas, 33 cortical thickness values, and six subcortical volumes), in which edge weights were proportional to the similarity between two brain morphological features in terms of deviation from healthy controls (i.e. *z*-score transformed). Global networks were characterized using measures of network segregation (clustering and modularity), network integration (global efficiency), and their balance (small-worldness), and their community membership was assessed. Hub profiling of regional networks was undertaken using measures of betweenness, closeness, and eigenvector centrality. Individually calculated network measures were integrated across the 37 datasets using a meta-analytical approach. These network measures were summated across the network density range of $K = 0.10–0.25$ per participant, and were integrated across the 37 datasets using a meta-analytical approach.

Received June 11, 2019. Revised November 24, 2019. Accepted November 26, 2019

Compared with healthy controls, at a global level, the structural covariance networks of OCD showed lower clustering ($P < 0.0001$), lower modularity ($P < 0.0001$), and lower small-worldness ($P = 0.017$). Detection of community membership emphasized lower network segregation in OCD compared to healthy controls. At the regional level, there were lower (rank-transformed) centrality values in OCD for volume of caudate nucleus and thalamus, and surface area of paracentral cortex, indicative of altered distribution of brain hubs. Centrality of cingulate and orbito-frontal as well as other brain areas was associated with OCD illness duration, suggesting greater involvement of these brain areas with illness chronicity. In summary, the findings of this study, the largest brain structural covariance study of OCD to date, point to a less segregated organization of structural covariance networks in OCD, and reorganization of brain hubs. The segregation findings suggest a possible signature of altered brain morphometry in OCD, while the hub findings point to OCD-related alterations in trajectories of brain development and maturation, particularly in cingulate and orbitofrontal regions.

1 Seoul National University Hospital, Seoul, Republic of Korea
2 Yeongeon Student Support Center, Seoul National University College of Medicine, Seoul, Republic of Korea
3 Amsterdam UMC, Vrije Universiteit Amsterdam, Department of Psychiatry, Amsterdam Neuroscience, Amsterdam, The Netherlands
4 Amsterdam UMC, Vrije Universiteit Amsterdam, Department of Anatomy & Neurosciences, Amsterdam Neuroscience, Amsterdam, The Netherlands
5 Imaging Genetics Center, Mark and Mary Stevens Neuroimaging & Informatics Institute, Keck School of Medicine of the University of Southern California, Marina del Rey, CA, USA
6 Department of Psychiatry, Graduate School of Medical Science, Kyoto Prefectural University of Medicine, Kyoto, Japan
7 The Margaret and Wallace McCain Centre for Child, Youth & Family Mental Health, Campbell Family Mental Health Research Institute, The Centre for Addiction and Mental Health, Department of Psychiatry, Faculty of Medicine, University of Toronto, Toronto, Canada
8 Centre for Brain and Mental Health, The Hospital for Sick Children, Toronto, Canada
9 Department of Psychiatry, Yale University School of Medicine, New Haven, Connecticut, USA
10 Mathison Centre for Mental Health Research and Education, Hotchkiss Brain Institute, Cumming School of Medicine, University of Calgary, Calgary, Alberta, Canada
11 Department of Psychiatry, Cumming School of Medicine, University of Calgary, Calgary, Alberta, Canada
12 Departamento e Instituto de Psiquiatria do Hospital das Clinicas, IPQ HCFMUSP, Faculdade de Medicina, Universidade de Sao Paulo, SP, Brazil
13 Psychiatry and Clinical Psychobiology, Division of Neuroscience, Scientific Institute Ospedale San Raffaele, Milano, Italy
14 Department of Psychology, Humboldt-Universität zu Berlin, Berlin, Germany
15 Obsessive-Compulsive Disorder (OCD) Clinic Department of Psychiatry National Institute of Mental Health and Neurosciences, Bangalore, India
16 Department of Child and Adolescent Psychiatry and Psychotherapy, Psychiatric Hospital, University of Zurich, Zurich, Switzerland
17 Magnetic Resonance Image Core Facility, IDIBAPS (Institut d'Investigacions Biomèdiques August Pi i Sunyer), Barcelona, Spain
18 Department of Psychiatry, First Affiliated Hospital of Kunming Medical University, Kunming, China
19 Institute of Human Behavioral Medicine, SNU-MRC, Seoul, Republic of Korea
20 Laboratory of Neuropsychiatry, Department of Clinical and Behavioral Neurology, IRCCS Santa Lucia Foundation, Rome, Italy
21 Amsterdam UMC, University of Amsterdam, Department of Psychiatry, Amsterdam Neuroscience, Amsterdam, The Netherlands
22 Netherlands Institute for Neuroscience, Royal Netherlands Academy of Arts and Sciences, Amsterdam, The Netherlands
23 Semel Institute for Neuroscience and Human Behavior, University of California, Los Angeles, CA, USA
24 SAMRC Unit on Risk and Resilience in Mental Disorders, Department of Psychiatry, University of Cape Town, Cape Town, South Africa
25 Centro de Investigación Biomédica en Red de Salud Mental (CIBERSAM), Carlos III Health Institute, Barcelona, Spain
26 Department of Psychiatry, Bellvitge University Hospital, Bellvitge Biomedical Research Institute-IDIBELL, L'Hospitalet de Llobregat, Barcelona, Spain
27 Shanghai Mental Health Center Shanghai Jiao Tong University School of Medicine, PR China
28 De Bascule, Academic Center for Child and Adolescent Psychiatry, Amsterdam, The Netherlands
29 Amsterdam UMC, Department of Child and Adolescent Psychiatry, Amsterdam, The Netherlands
30 Department of Neuropsychiatry, Graduate School of Medical Sciences, Kyushu University, 3-1-1 Maidashi Higashi-ku, Fukuoka, Japan
31 Department of Neuroradiology, Klinikum rechts der Isar, Technische Universität München, Germany
32 TUM-Neuroimaging Center (TUM-NIC) of Klinikum rechts der Isar, Technische Universität München, Germany
33 Department of Child and Adolescent Psychiatry and Psychology, Institute of Neurosciences, Hospital Clínic Universitari, Barcelona, Spain
34 Institut d'Investigacions Biomèdiques August Pi i Sunyer (IDIBAPS), Barcelona, Spain
35 Department of Medicine, University of Barcelona, Barcelona, Spain
36 Centro de Investigación Biomèdica en Red de Salud Mental (CIBERSAM), Barcelona, Spain
37 SAMRC Unit on Anxiety and Stress Disorders, Department of Psychiatry, University of Stellenbosch, South Africa

38 Life and Health Sciences Research Institute (ICVS), School of Medicine, University of Minho, Braga, Portugal
39 Columbia University Medical College, Columbia University, New York, NY, USA
40 The New York State Psychiatric Institute, New York, NY, USA
41 Department of Psychiatry, Bellvitge University Hospital, Bellvitge Biomedical Research Institute-IDIBELL, L'Hospitalet de Llobregat, Barcelona, Spain
42 Department of Clinical Sciences, University of Barcelona, Spain
43 Department of Clinical Neuroscience, Centre for Psychiatry Research, Karolinska Institutet, Stockholm, Sweden
44 McMaster University, Department of Psychiatry and Behavioural Neurosciences, Hamilton, Ontario, Canada
45 Clinical Academic Center–Braga, Braga, Portugal
46 ICVS-3Bs PT Government Associate Laboratory, Braga, Portugal
47 Department of Neuropsychiatry, Graduate School of Medical Sciences, Kyushu University, Fukuoka, Japan
48 Division of Child and Adolescent Psychiatry, University of California, Los Angeles, CA, USA
49 Center for Mathematics, Computing and Cognition, Universidade Federal do ABC, Santo Andre, Brazil
50 Center for OCD and Related Disorders, New York State Psychiatric Institute, New York, NY, USA
51 Pediatric OCD Consultation Service, Anxiety Treatment and Research Center, St. Joseph's HealthCare, Hamilton, Ontario, Canada
52 Department of Psychobiology and Methodology of Health Sciences, Universitat Autònoma de Barcelona, Spain
53 Beth K. and Stuart C. Yudofsky Division of Neuropsychiatry, Department of Psychiatry and Behavioral Sciences, Baylor College of Medicine, Houston, Texas, USA
54 Yale University School of Medicine, New Haven, Connecticut, USA
55 Clinical Neuroscience and Development Laboratory, Olin Neuropsychiatry Research Center, Hartford, Connecticut, USA
56 Icahn School of Medicine at Mount Sinai, New York, USA
57 James J. Peters VA Medical Center, Bronx, New York, USA
58 Institute of Living/Hartford Hospital, Hartford, Connecticut, USA
59 Shanghai Key Laboratory of Psychotic Disorders, PR China
60 Department of Psychiatry, The First Affiliated Hospital of Kunming Medical University, Kunming, Yunnan, PR China
61 Department of Psychiatry, Seoul National University College of Medicine, Seoul, Republic of Korea
62 Department of Brain and Cognitive Sciences, Seoul National University College of Natural Sciences, Seoul, Republic of Korea

Correspondence to: Prof Jun Soo Kwon
Department of Psychiatry, Seoul National University College of Medicine, 101, Daehak-ro,
Jongno-gu, Seoul 03080, Republic of Korea
E-mail: kwonjs@snu.ac.kr

Keywords: brain structural covariance network; graph theory; obsessive-compulsive disorder; pharmacotherapy; illness duration

Abbreviation: OCD = obsessive-compulsive disorder

Introduction

Three decades of neuroimaging research support the view that structural brain abnormalities in obsessive-compulsive disorder (OCD) do not merely involve alterations in discrete brain regions, but rather are best characterized in terms of altered networks of brain structures (Boedhoe *et al.*, 2017). More specifically, brain-based models of OCD have emphasized the role of the cortico-striato-thalamo-cortical loops and have also suggested the involvement of fronto-limbic, fronto-parietal and cerebellar regions (Menzies *et al.*, 2008; Milad and Rauch, 2012; de Wit *et al.*, 2014; Piras *et al.*, 2015; van den Heuvel *et al.*, 2016; Boedhoe *et al.*, 2017, 2018; Fouche *et al.*, 2017). Most studies of brain networks in OCD have used resting state functional MRI (rs-fMRI) (Soriano-Mas and Harrison, 2017; Gürsel *et al.*, 2018), with alterations evident in intra-network connections of fronto-limbic and fronto-striatal networks (Anticevic *et al.*, 2014; Gottlich *et al.*, 2014; Posner *et al.*, 2014; Armstrong *et al.*, 2016; de Vries *et al.*, 2017; Takagi *et al.*, 2017). Furthermore, a meta-analysis of rs-fMRI studies comparing OCD to healthy controls found decreased intra-network connectivity of the fronto-parietal and salience networks, as well as reduced inter-network connectivity between the salience, fronto-parietal and default-mode networks (Gürsel *et al.*, 2018).

Brain structural covariance networks reflect intra-individual (Yun *et al.*, 2016; Seidlitz *et al.*, 2018*a*) or inter-individual (Alexander-Bloch *et al.*, 2013; Kaczkurkin *et al.*, 2019; Wannan *et al.*, 2019) covariation in morphology of different brain areas, which may in turn point to common trajectories in brain development and maturation (Yun *et al.*, 2015, 2016; Hunt *et al.*, 2016). Such networks may focus on a range of morphological features including regional brain volume (Spreng *et al.*, 2019), cortical thickness (Solé-Casals *et al.*, 2019), cortical surface area (Sharda *et al.*, 2017), and cortical white-grey contrast (Makowski *et al.*, 2019), as well as the paired or conjoint patterns between different brain regions (Seidlitz *et al.*, 2018*b*; Hoagey *et al.*, 2019) Brain structural covariance has been estimated using Pearson's correlation coefficient (Seidlitz *et al.*, 2018*a*; Solé-Casals *et al.*, 2019; Wannan *et al.*, 2019), partial least squares (Hoagey *et al.*, 2019; Spreng *et al.*, 2019), non-negative matrix factorization (Kaczkurkin *et al.*, 2019), and inverse exponential of

the difference between *z*-score transformed brain morphological values (Wee *et al.*, 2013; Yun *et al.*, 2015, 2016), among others. Structural covariance networks are more similar to patterns of functional connectivity than the architecture of white matter connections, suggesting that areas that co-vary in morphological characteristics also belong to the same functional network (Zielinski *et al.*, 2010; Soriano-Mas *et al.*, 2013). Such networks are thought to be shaped by genetic and environmental influences from early childhood (Richmond *et al.*, 2016) and may continue to be reshaped during the lifespan (Alexander-Bloch *et al.*, 2013; Aboud *et al.*, 2019; Qi *et al.*, 2019) by a range of trophic influences (Ferrer *et al.*, 1995; Draganski *et al.*, 2004; Mechelli *et al.*, 2005).

Inter-individual brain structural covariance networks have been explored in a few studies of OCD and healthy controls. For example, Pujol *et al.* (2004) found a negative association between relative volume reduction for OCD (compared to healthy controls) in the medial prefrontal-insulo-opercular cortical regions and relative volume enlargement of ventral striatum, suggesting that abnormal brain morphology in OCD might be distributed in coordinated fashion across diverse brain regions. In addition, a recent mega-analysis found higher covariance between volumes of left putamen and left frontal operculum, and higher covariance between volumes of right amygdala and ventromedial prefrontal cortex in OCD compared to healthy controls (Subira *et al.*, 2016). Further, local cortical gyrification (associated with cortical maturation)-based structural covariance network demonstrated lower covariance among mainly ventral brain regions in OCD compared to healthy controls (Reess *et al.*, 2018*b*). However, few studies have explored intra-individual brain structural covariance networks in OCD; consequently our understanding of the factors that influence changes in global and regional network characteristics within individuals with OCD is limited.

The ENIGMA-OCD Working Group has collaborated on developing a large database of structural brain imaging in OCD and healthy controls, providing a unique opportunity to undertake such an exploration. Here we constructed intra-individual structural covariance networks from region of interest-based brain morphological features using 37 datasets worldwide ($n = 1616$ for OCD; $n = 1463$ for healthy controls), and investigated network topology using a graph theory approach. The current study aimed to capture the intra-individual distribution of brain morphological changes (Wee *et al.*, 2013; Yun *et al.*, 2015, 2016) in OCD across 33 cortical surface areas, 33 cortical thickness values, and six subcortical volumes (Kremen *et al.*, 2013; Amlien *et al.*, 2016; Sussman *et al.*, 2016; Vijayakumar *et al.*, 2016; Krongold *et al.*, 2017; Schmaal *et al.*, 2017). Thus edge weights of the intra-individual structural covariance networks were estimated in proportion to the similarity between two brain morphological features in terms of deviation from healthy controls (i.e. *z*-score transformed). Networks were characterized at the global level using measures of network segregation (clustering coefficient and modularity), network integration (global efficiency), and their balance (small-worldness), as well as at the regional level using betweenness, closeness, and eigenvector centralities (Lancichinetti and Fortunato, 2009; Rubinov and Sporns, 2010; Cao *et al.*, 2016; Palaniyappan *et al.*, 2016; Vriend *et al.*, 2018). For preservation of the network edge weights-related information in the derived graph metrics, the global and regional graph metrics were summed across the network density range of $K = 0.10–0.25$ (Uehara *et al.*, 2014).

Previous neuroimaging studies of global network metrics have reported more (Zhang *et al.*, 2011, 2014), less (Shin *et al.*, 2014; Armstrong *et al.*, 2016; Jung *et al.*, 2017; Reess *et al.*, 2018*a*), or similar levels (Reess *et al.*, 2016) of segregated organization of white matter-based structural connectivity networks, resting state functional connectivity networks, or local gyrification index-based structural covariance networks in individuals with OCD, compared to healthy controls. These inconsistent findings raise the need for larger-scale meta-analysis. Therefore, the current study aimed to assess the level of global network segregation, as determined by the global clustering coefficient, using the largest dataset of structural covariance networks in OCD to date.

Materials and methods

Samples

This study included 37 datasets from 26 international research institutes participating in the OCD Working Group of the ENIGMA (Enhancing NeuroImaging and Genetics through Meta-Analysis) Consortium used in the meta-analytic between-group comparisons of OCD and healthy controls in terms of the subcortical volumes (Boedhoe *et al.*, 2017), cortical surface area and cortical thickness (Boedhoe *et al.*, 2018), in addition to the cortical and subcortical asymmetry (Kong *et al.*, 2019). Each dataset included demographic and neuroimaging data from OCD and healthy controls, as well as OCD clinical data (Table 1 and Supplementary material). The diagnosis of psychiatric disorders including OCD and other comorbid disorders (if any) was made using a structured or semi-structured interview; the Structured Clinical Interview for DSM-IV [SCID-I (First *et al.*, 2002); $n = 23$ datasets], the Mini-International Neuropsychiatric Interview [MINI (Sheehan *et al.*, 1998); $n = 6$ datasets], the Anxiety Disorder Interview Schedule [ADIS (Silverman *et al.*, 2001; Grisham *et al.*, 2004); $n = 2$ datasets], or the Schedule for Affective Disorders and Schizophrenia for School-Aged Children: Present and Lifetime Version [K-SADS-PL (Kaufman and Schweder, 2003); $n = 7$ datasets] (Table 1 and Supplementary material). Comorbid lifetime depressive disorder was present in 256 individuals with OCD, and comorbid lifetime anxiety disorder was present in 267 (Table 1 and Supplementary material). At the time of MRI acquisition, 721

Table 1 Demographic and clinical information

Study	Study PI	Study site	MRI field strength, T	Total, *n*		Age, mean (SD)		Sex, male / female		Comorbid lifetime depression (OCD) *n* (%)	Comorbid lifetime anxiety (OCD) *n* (%)	Y-BOCS total (OCD), mean (SD)	Medicated OCD, *n* (%)	Illness duration (OCD), mean (SD)
				HC	OCD	HC	OCD	HC	OCD					
1	Beucke	Berlin, GER	1.5	54	57	32 (11)	33 (11)	23 / 31	31 / 26	11 (19)	6 (11)	20 (7)	23 (40)	16.2 (11)
2	Cheng	Kunming, CHN	1.5	28	16	32 (8)	32 (12)	8 / 20	5 / 11	4 (25)	6 (38)	31 (7)	10 (63)	4.2 (5.2)
3	van den Heuvel	Amsterdam, NLD	1.5	35	37	31 (8)	35 (9)	12 / 23	11 / 26	11 (30)	6 (16)	23 (6)	0 (0)	20 (11.8)
4	Hoexter	San Paulo, BRA	1.5	9	38	28 (6)	31 (9)	5 / 4	17 / 21	20 (53)	24 (63)	28 (6)	8 (21)	17.4 (10.3)
5	Kwon	Seoul, KOR_01	1.5	103	45	24 (4)	25 (5)	57 / 46	34 / 11	0 (0)	0 (0)	20 (6)	11 (24)	7.3 (5.2)
6	Kwon	Seoul, KOR_02	1.5	45	34	25 (5)	29 (7)	29 / 16	19 / 15	1 (3)	0 (0)	24 (6)	0 (0)	9.9 (7.1)
7	Mataix-Cols	Stockholm, SWE	1.5	28	34	36 (11)	39 (11)	9 / 19	15 / 19	9 (26)	9 (26)	25 (8)	14 (41)	20.5 (14.9)
8	Menchon	Barcelona, ESP	1.5	55	95	32 (10)	35 (9)	22 / 33	47 / 48	15 (16)	19 (20)	25 (6)	91 (96)	13.9 (9.9)
9	Morgado	Braga, Portugal	1.5	51	58	28 (6)	27 (8)	19 / 32	27 / 31	–	–	26 (6)	58 (100)	–
10	Nakamae	Kyoto, JPN	1.5	48	81	30 (8)	32 (9)	25 / 23	37 / 44	18 (22)	8 (10)	25 (6)	39 (48)	6.7 (6.8)
11	Reddy	India	1.5	20	29	26 (6)	28 (7)	14 / 6	16 / 13	–	–	25 (9)	0 (0)	5.7 (5.3)
12	Benedetti	Milan, ITA	3	23	22	29 (11)	35 (11)	19 / 4	13 / 9	0 (0)	0 (0)	31 (6)	13 (59)	18.7 (12)
13	Cheng	Kunming, CHN	3	72	40	26 (4)	33 (11)	20 / 52	21 / 19	13 (33)	37 (93)	28 (6)	25 (63)	5.4 (5.8)
14	Denys	Amsterdam, NLD	3	15	14	38 (12)	34 (11)	6 / 9	1 / 13	4 (29)	1 (7)	27 (6)	9 (64)	14.9 (13.5)
15	van den Heuvel	Amsterdam, NLD	3	30	32	39 (11)	39 (11)	12 / 18	16 / 16	17 (53)	13 (41)	21 (6)	0 (0)	25.9 (12.9)
16	Koch	Munchen, GER	3	71	75	30 (9)	31 (10)	28 / 43	28 / 47	0 (0)	0 (0)	21 (6)	45 (60)	14.3 (10.6)
17	Kwon	Seoul, KOR	3	89	90	26 (7)	27 (7)	54 / 35	56 / 34	2 (2)	1 (1)	27 (7)	2 (2)	7.7 (6.7)
18	Nakamae	Kyoto, JPN	3	39	34	30 (7)	33 (10)	19 / 20	12 / 22	7 (21)	3 (9)	22 (7)	0 (0)	8.1 (6.1)
19	Nakao	Fukuoka, JPN	3	31	66	39 (13)	37 (10)	11 / 20	30 / 36	22 (33)	0 (0)	23 (6)	59 (89)	12.2 (9.3)
20	Nurmi	Los Angeles, USA	3	22	45	31 (12)	34 (11)	14 / 8	22 / 23	9 (20)	16 (36)	25 (4)	12 (27)	23 (10.8)
21	Reddy	India	3	139	201	26 (5)	30 (7)	86 / 53	107 / 94	31 (15)	15 (7)	26 (6)	82 (41)	7.3 (5.4)
22	Simpson	New York, USA	3	31	30	28 (8)	30 (8)	17 / 14	17 / 13	10 (33)	7 (23)	26 (4)	0 (0)	15.1 (8.7)
23	Spalletta	Rome, ITA	3	95	71	38 (11)	36 (11)	54 / 41	45 / 26	8 (11)	8 (11)	23 (9)	65 (92)	16.6 (11.4)
24	Stein	Cape Town, ZAF	3	25	21	31 (11)	31 (11)	10 / 15	11 / 10	0 (0)	0 (0)	23 (4)	9 (43)	17.9 (11.3)
25	Tolin	Conneticut, USA	3	32	27	48 (12)	32 (12)	7 / 25	18 / 9	11 (41)	12 (44)	23 (5)	21 (78)	–
26	Walitza	Zurich, CHE	3	15	13	33 (9)	31 (7)	4 / 11	7 / 6	6 (46)	7 (54)	18 (10)	6 (46)	12.8 (10)
27	Wang	Shanghai, CHN	3	35	47	26 (8)	30 (9)	18 / 17	23 / 24	0 (0)	0 (0)	25 (5)	0 (0)	6.5 (5.5)
28	Lazaro	Barcelona, ESP	1.5	29	29	15 (2)	14 (2)	14 / 15	18 / 11	0 (0)	5 (17)	22 (6)	15 (52)	2.1 (1.8)
29	Arnold	Ontario, CAN	3	11	34	12 (2)	13 (2)	6 / 5	20 / 14	7 (21)	10 (29)	21 (8)	21 (62)	4.2 (2.6)
30	Gruner	Conneticut, USA	3	17	10	14 (2)	15 (2)	8 / 9	9 / 1	2 (20)	6 (60)	27 (5)	6 (60)	–
31	Hoexter	San Paulo, BRA	3	26	27	12 (2)	13 (2)	15 / 11	16 / 11	6 (22)	20 (74)	27 (5)	12 (44)	5.5 (2.4)
32	Huyser	Amsterdam, NLD	3	20	20	14 (3)	14 (2)	8 / 12	6 / 14	7 (35)	9 (45)	26 (5)	0 (0)	3.1 (2.6)
33	Lazaro	Barcelona, ESP	3	43	53	15 (2)	15 (2)	23 / 20	30 / 23	3 (6)	14 (26)	19 (7)	42 (79)	2.5 (2.1)
34	Nurmi	Los Angeles, USA	3	36	53	13 (2)	13 (3)	18 / 18	29 / 24	1 (2)	2 (4)	24 (4)	7 (13)	–
35	Reddy	India	3	10	14	14 (3)	14 (2)	5 / 5	8 / 6	1 (7)	3 (21)	22 (7)	12 (86)	1.5 (0.9)
36	Soreni	Ontario, CAN	3	20	18	11 (3)	13 (2)	10 / 10	7 / 11	0 (0)	0 (0)	23 (4)	0 (0)	–
37	Walitza	Zurich, CHE	3	11	6	16 (2)	16 (1)	6 / 5	5 / 1	0 (0)	0 (0)	18 (10)	4 (67)	5 (2.4)

A more detailed version of this table is provided in the Supplementary material. A dash indicates data were not available.

BRA = Brazil; CAN = Canada; CHE = Switzerland; CHN = China; ESP = Spain; GER = Germany; HC = healthy control; ITA = Italy; KOR_01/02 = South Korea site 1/2; NLD = the Netherlands; PI = principal investigator; SWE = Sweden; Y-BOCS = Yale–Brown Obsessive Compulsive Scale; ZAF = South Africa.

individuals with OCD were on psychotropic medication and 881 were not. Age of illness onset of OCD was 18.8 ± 9.1 years, and illness duration was 10.8 ± 10.1 years (n = 1415). Severity of obsessive-compulsive symptoms was assessed with the Yale-Brown Obsessive-Compulsive Scale (Y-BOCS; for patients aged ⩾18) or Children's Y-BOCS (CY-BOCS; for patients aged <18); the mean score of 24.2 ± 6.8 (n = 1581) indicated a moderate to severe range of symptoms in the study population. All local institutional review boards permitted the use of extracted numerical measures for meta-analysis.

Image acquisition and processing

Structural T_1-weighted brain MRI scans were acquired and processed at each study site. For acquisition parameters of each site see Supplementary Table 1. All parcellations were performed with fully automated segmentation software FreeSurfer version 5.3. (Fischl, 2012), following standardized ENIGMA protocols (http://enigma.usc.edu/protocols/imaging-protocols/). To ensure quality control, we visually inspected the segmentations of 68 (34 left and 34 right) cortical grey matter regions and seven subcortical regions based on the Desikan-Killiany atlas (Desikan *et al.*, 2006) and statistically evaluated the data for outliers (Boedhoe *et al.*, 2017, 2018). We excluded the volume values of bilateral entorhinal cortices and the nucleus accumbens because of segmentation issues (as calculation of intra-individual brain structural covariance networks requires every region of interest to be adequately measured in each participant; inclusion of regions of interest with relatively poorer quality segmentations would effectively decrease sample size).

Intra-individual cortical-subcortical structural covariance networks

As illustrated at 'step 1' in Fig. 1, bilaterally-averaged values (where brain regions were poorly segmented in one hemisphere, the value from the contralateral hemisphere was used as a proxy) of 33 cortical surface area regions of interest, 33 cortical thickness regions of interest, and six subcortical volume regions of interest, were corrected for age, sex, and individual brain size (Vuoksimaa *et al.*, 2016) per dataset (n = 37). The resulting residuals were then z-score transformed using mean and SD values of each region of interest calculated from healthy controls (to derive the degrees of brain morphological variations per region of interest relative to the 'average healthy controls' values). Finally, a measure of joint variation (which is not the same as the classical statistical definition of covariance) between the 72 morphometric features (33 cortical surface area values, 33 cortical thickness values, and six subcortical values) represented the edge-weights (distributed between 0 and 1) of the network and was calculated using the following formula (Yun *et al.*, 2015, 2016):

[Intra-individual brain structural covariance (joint variation) between the *ith* (for i = 1 to 72) and *j-th* (for j = 1 to 72) regions of interest in the *k-th* (for k = 1 to 'total number of participants per dataset') participant] = $1/\exp\{[(z\text{-transformed value of } i\text{-th region of interest in } k\text{-th participant}) - (z\text{-transformed value of } j\text{-th region of interest in } k\text{-th participant})]^2\}$ (1)

Graph theory approach: single subject level

Global network characteristics

Intra-individual structural covariance networks were thresholded (using 'threshold_proportional.m' function in network density range of K = 0.05–0.30; with interval of 0.01) and binarized (using the 'weight-conversion.m' function; e.g. when we applied a density threshold of K = 0.10, the edge weights in the network were sorted into numerical order and a cut-off was applied to retain only the strongest 10% of edges with edge weights converted to '1' and edges weights for other remaining edges becomes '0' (Fig 2, steps 2A and 3A). From these thresholded and binarized networks, four global metrics were determined: (i) global clustering (a tendency for brain regions to segregate into locally interconnected triplets of neighbouring nodes); (ii) global modularity (a measure of the segregation of the network into communities where nodes are more strongly connected with each other than nodes outside the community because of similar morphological characteristics; this measure is operationalized as the most frequently occurring value over 500 runs of estimation using 'modularity_und.m') (Newman, 2006; Reichardt and Bornholdt, 2006); (iii) global efficiency (how well on average each node is connected to all others based on the minimum number of steps nodes are separated from each other); and (iv) small-worldness (a measure of balance between the degree of segregation versus integration in brain network) using the Brain Connectivity Toolbox (Rubinov and Sporns, 2010) in MATLAB R2017a (Weinberg *et al.*, 2016; Das *et al.*, 2018; Zaremba *et al.*, 2018).

Among the diverse network density levels of K = 0.05–0.30 (with density interval of 0.01), only in the narrower network density levels of K = 0.10–0.25, three criteria of (Uehara *et al.*, 2014) (i) network connectedness (> 80% of nodes remain connected to other nodes within the network); (ii) modular organization (modularity > 0.3); and (iii) small-world organization (small-worldness > 1) were satisfied for >95% of the intra-individual structural covariance networks comprising each dataset (n = 37). Therefore, these network density levels of K = 0.10–0.25 (density interval = 0.01) were selected for the between-group comparison of global network characteristics, community membership detection, and hub profiling using the regional network characteristics (Fig. 2, step 3A). Estimation of the global network characteristics was done using Brain Connectivity Toolbox (https://www.nitrc.org/projects/bct/) in MATLAB R2017a.

Detection of community membership

In addition, we assessed community membership (Fortunato, 2010) for each structural covariance (joint variation) network. For thresholded (K = 0.10–0.25) and binarized intra-individual structural covariance (joint variation) networks, detection of communities [i.e. densely connected subgroups of nodes in a network (Power *et al.*, 2013)] was conducted using the InfoMap algorithm (Rosvall and Bergstrom, 2007; Fortunato, 2010; Power *et al.*, 2011; Kawamoto and Rosvall, 2015). First, a participant-level co-classification matrix (Dwyer *et al.*, 2014) that represented the fraction of network density level, in which each pair of nodes was clustered into the same community according to the InfoMap algorithm (Rosvall and Bergstrom, 2007; Kawamoto and Rosvall, 2015), was generated. Second, the

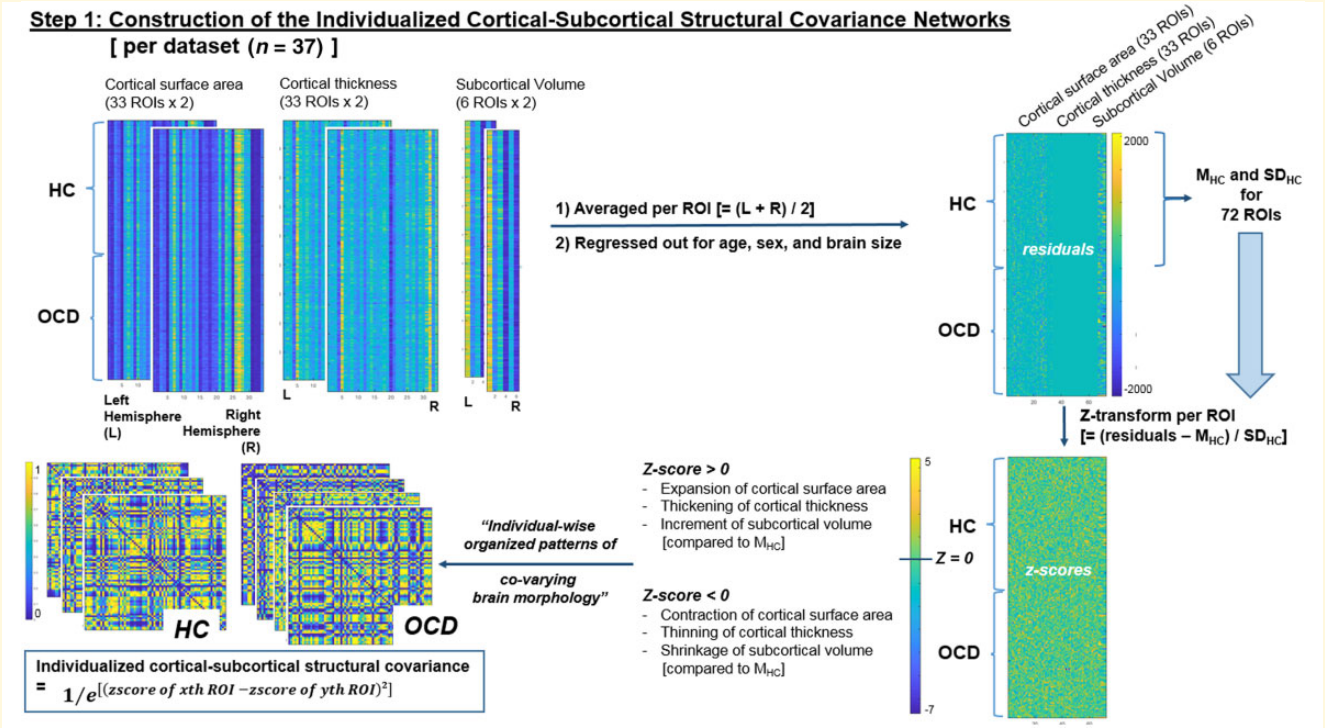

Figure 1 Schematic description of the study procedures: construction of intra-individual brain structural covariance networks. HC = healthy controls; L = left; M = mean; R = right; ROI = region of interest; SD = standard deviation.

InfoMap algorithm was applied to this co-classification matrix to generate a participant-level consensus of community membership (Fornito *et al.*, 2016). All procedures other than the InfoMap-based community estimation were done using MATLAB R2017a software (https://kr.mathworks.com).

Hub profiling and regional network characteristics

Principal brain regions that could be essential indicators of brain morphological changes within the network were assessed using hub profiling, which provided three local network measures: (i) betweenness centrality (the frequency of a node being located in the shortest path for each pair of two other nodes in a network); (ii) closeness centrality (the ease with which one node can reach all other nodes within a network); and (iii) eigenvector centrality (a self-referential measure of centrality that reflects the presence of connectedness of one node to other nodes with high eigenvector centrality) (Rubinov and Sporns, 2010) (Fig 2, step 2B). As distribution of these local network measures does not follow normal distribution in a scale-free network, prior to the between-group comparison and meta-analysis, these regional centrality metrics were rank-transformed using the 'tiedrank.m' function of MATLAB R2017a and were averaged in the network density range of $K = 0.10–0.25$ to be re-ranked at participant-level; participant-level hubs were selected as top-10 ranked nodes in two or three centralities. All of the procedures described above were conducted using the Brain Connectivity Toolbox (Rubinov and Sporns, 2010) and MATLAB R2017a software (https://kr.mathworks.com).

Meta-analysis of graph metrics

Global network characteristics

Meta-analysis of between-group differences in global network characteristics across the whole dataset ($n = 37$; Fig. 2, step 3A) was performed using a random-effects meta-analytic model (Hedges and Vevea, 1998; Kambeitz *et al.*, 2016) incorporating the bias-corrected standardized mean difference (SMD = Hedges' g) between OCD and healthy controls for each of the four global network characteristics (summated over the network density range of $K = 0.10–0.25$) that satisfied network connectedness, modular organization, and small-world organization; see 'Graph theory approach: single subject level' section). Summary effect sizes were calculated with restricted maximum-likelihood estimator (REML) (Raudenbush, 2009; Viechtbauer, 2010). Estimates for heterogeneity were assessed with the I^2 value (Raudenbush, 2009). For all analyses, a significance level of $P < 0.01$ was used, i.e. $P < 0.05/5$ number of global network characteristics (= 4) plus local network-related measure of the Dice coefficient (= 1; see section below) (Kambeitz *et al.*, 2016). All statistical analyses were conducted using the R package 'metafor' version 2.0.0 (Viechtbauer, 2010).

Community membership

First, summation of network-transformed community profiles for each individual provided dataset-level co-classification matrices (in which higher edge weights indicated that two nodes were clustered in the same community across a large proportion of participants in dataset) for OCD and for healthy controls (Fornito *et al.*, 2016). Second, consensus of community membership at dataset level (for OCD and healthy controls

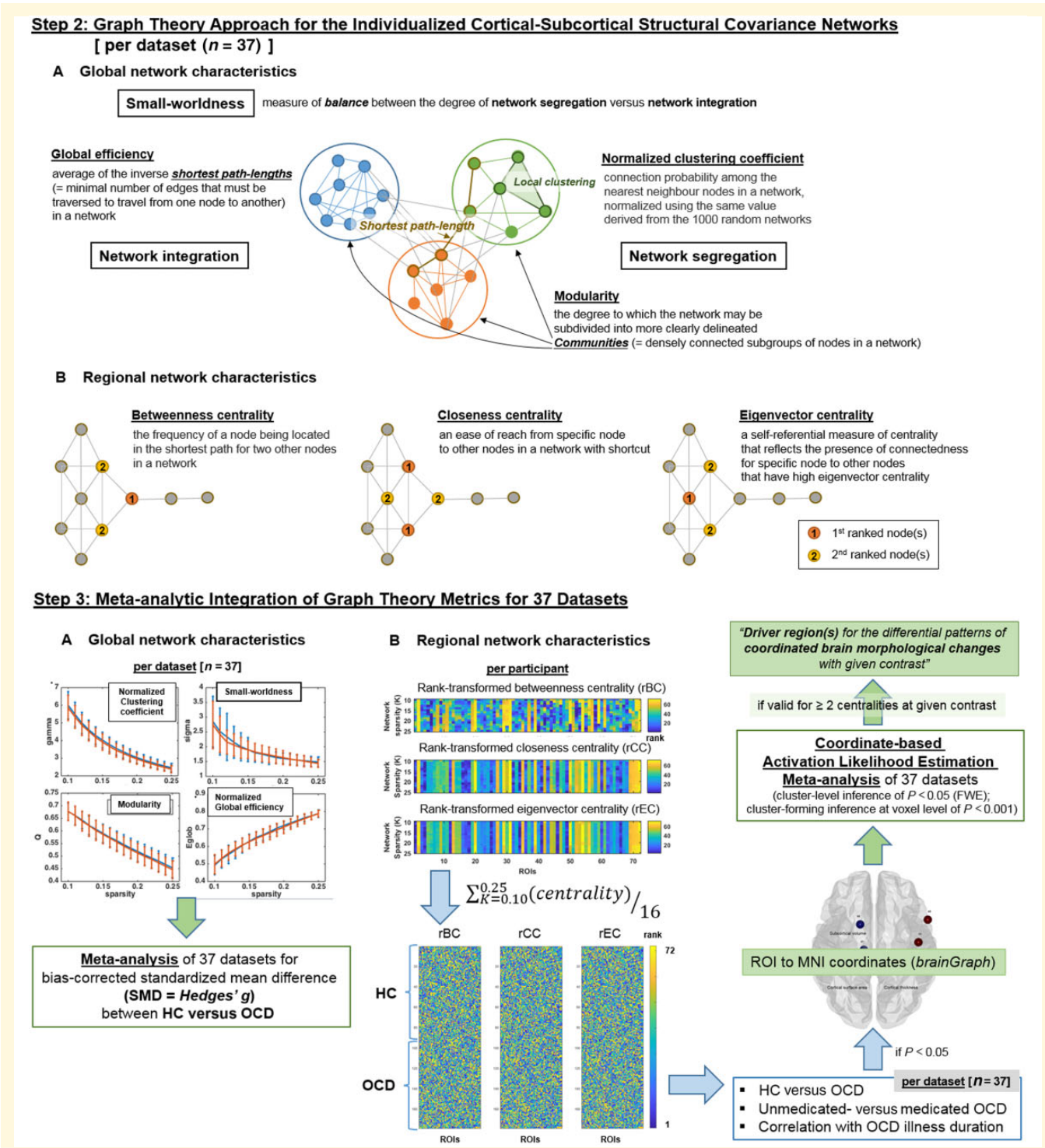

Figure 2 Schematic description of the study procedures. (**A**) Calculation of graph theory metrics from the intra-individual brain structural covariance networks at single-subject level and (**B**) meta-analytic integration of graph theory metrics for 37 datasets. HC = healthy controls; ROI = region of interest.

separately) was estimated by applying the InfoMap algorithm to the weighted and thresholded (at density level of $K = 0.10$) version of the dataset-level co-classification matrices. Third, dataset-level consensus community profiles of OCD and healthy controls were binarized, multiplied by the square root of participants number per dataset, and summed to generate the meta-analytic co-classification matrices of OCD or healthy controls ($n = 37$). Finally, a weighted and thresholded (at density level of $K = 0.10$) version of these meta-analytic co-classification matrices underwent InfoMap-based community detection, to

determine the meta-analytic consensus community profile for brain structural covariance networks of OCD and healthy controls. All procedures other than the InfoMap-based community estimation were performed using MATLAB R2017a.

Hub profiling and regional network characteristics

In the current study, hub profiling was done to find the principal brain regions that could be essential indicators of intra-individual distribution of brain morphological changes (= deviation from healthy controls) based on the three local metrics of betweenness, closeness, and eigenvector centralities (Fig. 2). Three rank-transformed centralities (betweenness, closeness, and eigenvector) were rank-transformed at the participant level, and were averaged in the network density range of $K = 0.10$–0.25. The top 10 ranked nodes (i.e. 10 nodes illustrated in Fig. 4 and Supplementary Fig. 1) for two or three centralities as calculated from the summation of participant-level centrality values within each dataset ($n = 37$) were classified as dataset-level hubs for OCD or healthy controls. Finally, meta-analytic hub scores for all network nodes (= 33 cortical surface area values + 33 cortical thickness values + six subcortical volumes) were calculated by summing the values of [(presence (= 1) or absence (= 0) of network nodes in the hub profile of each dataset) × (square root of participants number per dataset)] across the whole dataset ($n = 37$) for OCD and healthy controls separately; top-10 ranked nodes for this meta-analytic hub score were defined as meta-analytic hubs for OCD or healthy controls, respectively.

Between-group comparison of rank-transformed centrality values at the dataset level ($n = 37$) was performed using the Wilcoxon rank sum test. Nodes that showed statistically significant differences between OCD and healthy controls ($P < 0.05$) were recoded into MNI coordinates using *brainGraph* (https://cran.r-project.org/web/packages/brainGraph), and underwent coordinate-based meta-analysis, i.e. activation likelihood estimation (ALE), using *gingerALE* version 2.3.6. (Eickhoff *et al.*, 2017). In this ALE-based meta-analysis, nodes that showed significant effect sizes [cluster-level corrected threshold of $P < 0.05$ (family-wise error, FWE); cluster-forming threshold at voxel level of $P < 0.001$] for between-group differences in two or three centralities were considered valid (Fig. 2, step 3B).

Lastly, to explore the difference in hubs in terms of their topographical location between OCD and healthy controls, we also calculated the Dice similarity coefficient (Dice, 1945), a measure of the degree of overlap between each participant-level hub profile versus the reference (= hub profile of healthy controls per dataset). For meta-analysis, the bias-corrected SMD (Hedges' g) of Dice similarity coefficient (i) between the healthy controls and OCD (37 dataset) as well as (ii) between unmedicated OCD and medicated OCD (12 dataset in which >10 participants existed for all of the two subgroups) were calculated and entered into a random-effects meta-analytic model (Schmidt *et al.*, 2009; Kambeitz *et al.*, 2016). Summary effect sizes were calculated with REML (Raudenbush, 2009; Viechtbauer, 2010), and estimates for the amount of heterogeneity were assessed by way of the I^2 value (= the percentage of total variability across dataset that is due to heterogeneity than by chance) (Higgins *et al.*, 2003). For all analyses, a significance level of $P < 0.05$ (two-tailed) was used (Kambeitz *et al.*, 2016) and all statistical analyses were conducted using the R package 'metafor' version 2.0.0 (Viechtbauer, 2010).

Influence of comorbid lifetime depressive or anxiety disorders in patients with OCD

Thirty-five (of 37) datasets provided information about comorbid lifetime depressive and anxiety disorders in OCD individuals; meta-analysis of global network characteristics and Dice coefficients was conducted to assess between-group differences in (i) OCD with and without comorbid lifetime depressive disorder ($n = 10$ datasets, in which $n > 10$ for both OCD subgroups); and (ii) OCD with and without comorbid lifetime anxiety disorders ($n = 7$ datasets, in which $n > 10$ for both OCD subgroups).

Influence of medication

Twenty-seven (of 37) datasets provided information about medication status (= presence or absence of psychotropic medication prescribed at the time of MRI data acquisition) of OCD individuals; meta-analytic integration for the between-group comparison of regional network characteristics (= centralities) between medicated OCD versus unmedicated OCD was undertaken for these datasets. Furthermore, meta-analytic integration of between-group differences for global network metrics and Dice coefficients were conducted using results retrieved from 12 datasets (in which $n > 10$ for both medicated and unmedicated subjects).

Influence of OCD illness duration

Fisher's z-transformed correlation coefficients between the OCD illness duration and four global network metrics were calculated per dataset ($n = 32$ datasets). Each of these correlation coefficients per dataset and per global network characteristics were meta-analytically integrated using the same pipeline as for the global network characteristics. Likewise, Spearman correlation coefficients between the OCD illness duration and rank-transformed (betweenness, closeness, or eigenvector) centrality measures were also calculated per dataset. Meta-analysis of the dataset-level nodes that showed significant correlation with OCD illness duration ($P < 0.05$) was performed using using gingerALE version 2.3.6 [$P < 0.05$ (cluster-level FWE)] (Eickhoff *et al.*, 2017).

Data availability

De-identified data are available from the corresponding author upon reasonable request.

Results

Patients with OCD versus healthy controls

Demographic and clinical characteristics

A total of 37 datasets worldwide ($n = 1616$ for OCD; $n = 1463$ for healthy controls) were included in this study. Demographic and clinical characteristics for each dataset are described in Table 1 and Supplementary material. Between-group (OCD versus healthy controls) statistical tests for age (using the independent t-test) and sex ratio (using the

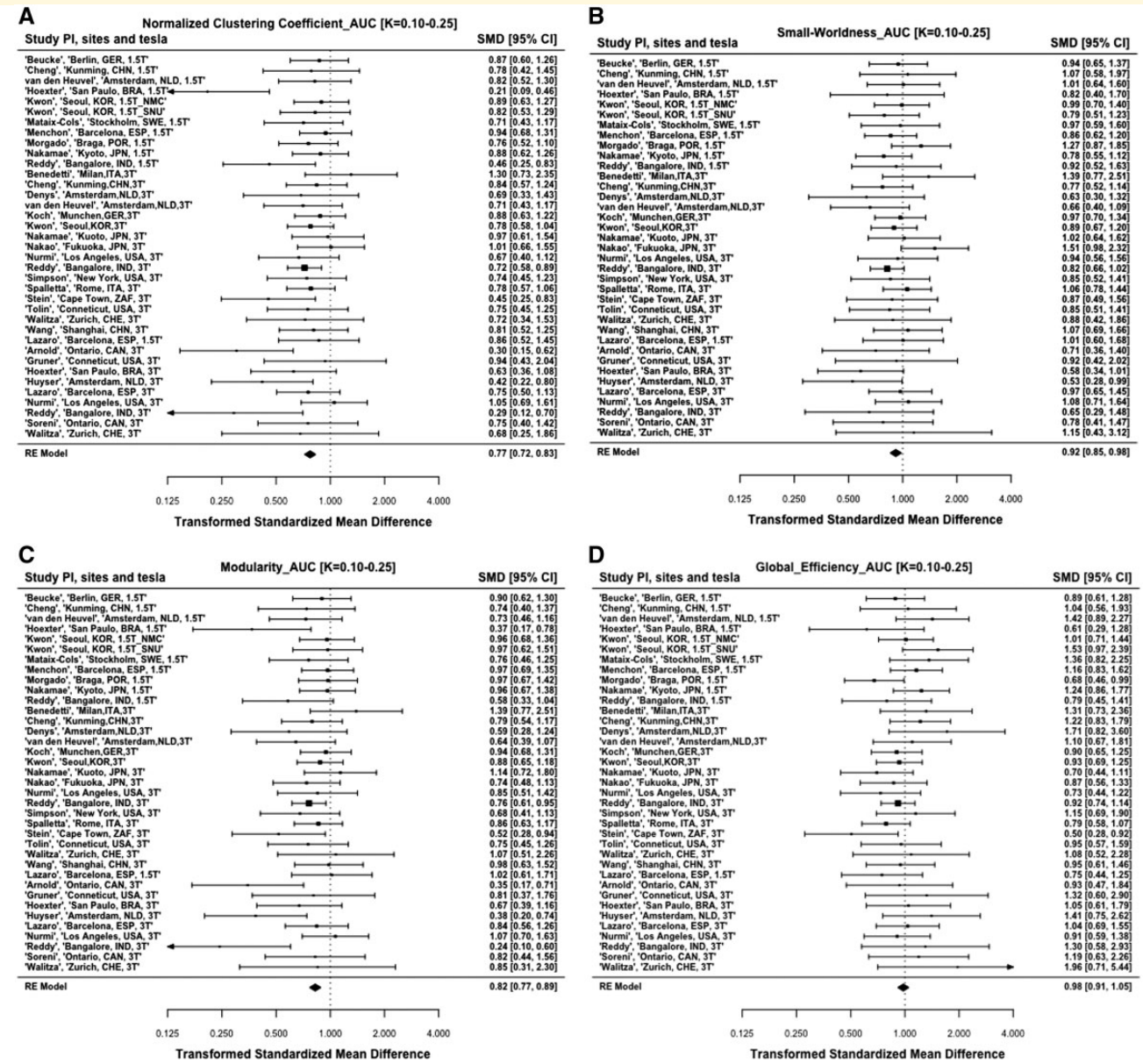

Figure 3 Forest plots of the meta-analysis of global graph metrics comparying the OCD and healthy control groups. (**A**) Global clustering, (**B**) small-worldness, (**C**) modularity, (**D**) global efficiency, and (**E**) dice similarity coefficient. HC = healthy controls; ROI = region of interest.

chi-squared test) did not show statistically significant differences between OCD and healthy controls ($P > 0.05$) for 31 (83.8%) and 34 datasets (91.9%), respectively. On the other hand, years of education (information available for 27 datasets) were fewer in OCD compared to healthy controls ($P < 0.05$) in 10 (27.0%) datasets.

Global network characteristics

Meta-analysis of global network characteristics for the intra-individual brain structural covariance networks (Table 2 and Fig. 3A–D) showed lowered global clustering and modularity in OCD compared to healthy controls (all P's < 0.01). Global efficiency and small-worldness did not differ significantly between OCD and healthy controls (all P's > 0.01). When the sample was divided into two groups (adults and adolescents), and analyses run in each, these findings continued to hold true (Table 2). Additional meta-analyses using years of education as a moderator did not show any significant influence of this variable (all P's > 0.05) on either the global network metrics of global clustering ($Q_m = 1.456$, $df = 2$, $P = 0.483$), modularity ($Q_m = 0.819$, $df = 2$, $P = 0.664$), global efficiency ($Q_m = 0.673$, $df = 2$, $P = 0.714$), and small-worldness ($Q_m = 0.139$, $df = 2$, $P = 0.933$), or on the Dice similarity coefficient ($Q_m = 1.447$, $df = 2$, $P = 0.485$).

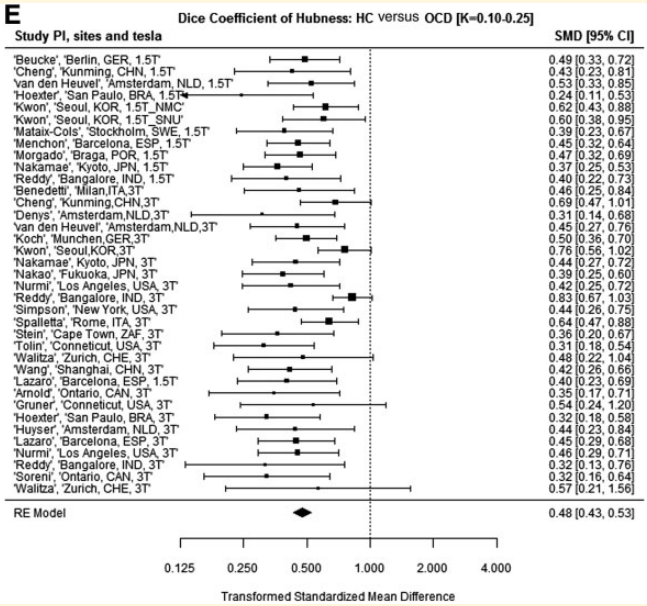

Figure 3 Continued

Community membership

Community membership analysis detected that the healthy controls network had six modules (or subgroups within the network), while the OCD network had three modules, indicative of less global network segregation. The six community modules of the healthy controls network (Fig. 4 and Supplementary Fig. 1) were module 1 [the principal (31 nodes); including six hubs of cortical surface area for medial orbitofrontal, caudal middle frontal, and parahippocampal cortices, as well as cortical thickness for posterior cingulate, pars triangularis, and insula], module 2 [cingulate-parietal-inferior frontal (13 nodes)], module 3 [subcortical (six nodes); including two hubs named pallidal and caudate volumes], module 4 [frontal pole-occipital (six nodes); including cortical thickness for cuneus as hub], module 5 [paracentral-temporal (six nodes); including a hub of paracentral cortical thickness], and module 6 [insula-perisylvian (five nodes)]. As smaller communities with less than four nodes (<5% of total nodes) were excluded, six nodes comprising module 2 for healthy controls [cortical surface area of caudal-rostral anterior cingulate and lateral orbitofrontal cortices, in addition to cortical thickness of paracentral, superior parietal, and supramarginal cortices] were not classified in these communities.

In contrast, community membership of individualized structural covariance networks for OCD (Fig. 4 and Supplementary Fig. 1) showed just three modules: module 1 [in which eight OCD hubs for cortical surface area of superior temporal sulcus (module 1 in healthy controls), posterior cingulate (module 2 in healthy controls), rostral middle frontal-insular-superior temporal (module 6 in healthy controls), and pericalcarine cortices, as well as cortical thickness of caudal anterior cingulate-frontal pole (module 1 in healthy controls) included], module 2 [comprising cortical thickness of inferior parietal lobule-precuneus (module 2 in healthy controls) in addition to cuneus-lingual-pericalcarine gyri (module 4 in healthy controls)], and module 3 (includes a hub named hippocampal volume).

Regional network characteristics

Of the 10 hubs for the OCD network (Fig. 4 and Supplementary Fig. 1), only one node, i.e. cortical thickness of postcentral cortex [member of the paracentral-temporal module in healthy controls; fifth community (red square) in Supplementary Fig. 1], was found among the 10 healthy controls hubs. Meta-analysis of Dice similarity coefficients showed lower Dice similarity coefficient in OCD compared to healthy controls (Table 2 and Fig. 3E), indicating that the nodes classified as hubs differed between OCD and healthy controls. In terms of the centralities, compared to healthy controls, rank-transformed centrality of caudate nucleus volume was lower in OCD (healthy controls hub; Fig. 5A and Supplementary Fig. 3).

Influence of comorbid lifetime depressive or anxiety disorders in patients with OCD

No significant differences in global network characteristics or Dice similarity coefficients were found between OCD with comorbid lifetime depression versus OCD without lifetime depression, nor between OCD with comorbid lifetime anxiety disorder versus OCD without lifetime anxiety disorder (Table 2).

Table 2 Meta-analysis of global network characteristics and Dice similarity coefficients

	logSMD	*k*	z	*P*-value	95% CI	I^2 (%)	Q	*P*
OCD versus HC								
Global clustering coefficient (total)	0.77	37	−6.94	<0.001	0.72 to 0.83	0.01	44.8	0.149
Adults (⩾18 years)	0.79	27	−5.89	<0.001	0.73 to 0.85	<0.001	26.8	0.418
Adolescents (<18 years)	0.66	10	−3.16	0.002	0.50 to 0.85	45.7	16.5	0.058
Modularity (total)	0.82	37	−5.21	<0.001	0.77 to 0.89	0.01	43.1	0.194
Adults (⩾18 years)	0.84	27	−4.28	<0.001	0.78 to 0.91	0.01	22.3	0.670
Adolescents (<18 years)	0.68	10	−2.63	0.009	0.51 to 0.91	54.0	19.1	0.025
Small-worldness (total)	0.92	37	−2.39	0.017	0.85 to 0.98	0.001	26.2	0.886
Adults (⩾18 years)	0.93	27	−1.82	0.069	0.86 to 1.01	<0.001	18.1	0.872
Adolescents (<18 years)	0.84	10	−1.82	0.068	0.70 to 1.01	<0.001	7.2	0.621
Global efficiency (total)	0.98	37	−0.54	0.586	0.91 to 1.05	0.02	38.5	0.358
Adults (⩾18 years)	0.97	27	−0.68	0.494	0.89 to 1.06	10.7	32.6	0.174
Adolescents (<18 years)	1.05	10	0.50	0.621	0.87 to 1.26	<0.001	5.3	0.809
Dice similarity coefficient (total)	0.48	37	−14.36	<0.001	0.43 to 0.53	39.35	58.3	0.011
Adults (⩾18 years)	0.49	27	−11.97	<0.001	0.44 to 0.55	45.7	49.6	0.004
Adolescents (<18 years)	0.41	10	−9.18	<0.001	0.34 to 0.50	<0.001	2.9	0.969
OCD patients with versus without lifetime comorbid depressive disorder								
Global clustering coefficient	0.89	10	−1.13	0.257	0.73 to 1.09	11.6	10.1	0.344
Modularity	0.90	10	−0.91	0.365	0.72 to 1.13	26.5	11.9	0.217
Small-worldness	0.96	10	−0.44	0.659	0.80 to 1.15	<0.001	6.6	0.678
Global efficiency	1.00	10	−0.04	0.966	0.83 to 1.20	<0.001	5.8	0.764
Dice similarity coefficient	1.04	10	0.32	0.751	0.84 to 1.28	21.4	13.2	0.155
OCD patients with versus without lifetime comorbid anxiety disorder								
Global clustering coefficient	0.99	7	−0.09	0.929	0.79 to 1.25	<0.001	5.1	0.531
Modularity	0.96	7	−0.39	0.695	0.76 to 1.20	<0.001	1.8	0.934
Small-worldness	1.00	7	0.01	0.993	0.79 to 1.27	3.1	6.6	0.357
Global efficiency	1.03	7	0.24	0.814	0.82 to 1.29	<0.001	6.2	0.403
Dice similarity coefficient	1.15	7	0.96	0.338	0.87 to 1.52	31.2	8.3	0.215
Medicated OCD versus unmedicated OCD								
Global clustering coefficient	0.95	12	−0.63	0.531	0.82 to 1.11	0.00	11.03	0.441
Modularity	0.94	12	−0.83	0.408	0.8 to 1.09	0.00	8.73	0.647
Small-worldness	0.99	12	−0.08	0.934	0.83 to 1.18	15.25	12.97	0.295
Global efficiency	0.85	12	−1.66	0.097	0.7 to 1.03	28.05	13.32	0.273
Dice similarity coefficient	1.06	12	0.72	0.474	0.91 to 1.24	2.16	6.90	0.807
	Correlation coefficient	***k***	**z**	***P*-value**	**95% CI**	I^2	**Q**	***P***
Illness duration in OCD								
Global clustering coefficient	−0.03	32	−0.85	0.393	−0.11 to 0.04	40.13	53.37	0.008
Modularity	−0.05	32	−1.32	0.188	−0.12 to 0.02	34.70	48.57	0.023
Small-worldness	−0.02	32	−0.67	0.584	−0.10 to 0.05	34.00	46.28	0.038
Global efficiency	−0.02	32	−0.59	0.558	−0.07 to 0.04	0.00	20.64	0.921

CI = 95% confidence interval; I^2 = total heterogeneity/total variability; *k* = number of studies included in given meta-analysis; log SMD = log-transformed standardized mean difference; *P* = *P*-value of heterogeneity test; *P*-value = *P*-value of random effect model (REML); Q = heterogeneity score; z = z-score.

Influence of medication for OCD

No significant differences in global network characteristics or Dice similarity coefficients were found between medicated and unmedicated OCD (Table 2). The structural covariance networks of healthy controls, medicated OCD, and unmedicated OCD demonstrated five, three, and two modules (or subgroups within the network), respectively (Supplementary Fig. 2).

Influence of OCD illness duration

OCD illness duration did not show significant correlations with global network characteristics (Table 2). However, OCD illness duration showed significant positive relationships with centrality (Fig. 5C and Supplementary Fig. 5) of cortical thickness for caudal anterior cingulate (OCD hub), cortical surface area for posterior cingulate (OCD hub), and cortical surface area of lateral orbitofrontal cortex (non-hub). Furthermore, OCD illness duration showed significant negative correlations with centrality of the cortical surface area for parahippocampal cortex (healthy control hub), cortical thickness for the frontal pole, cortical surface area for superior temporal and pericalcarine cortices (OCD hubs), cortical thickness for inferior parietal lobule, and cortical surface areas for inferior temporal and cingulate isthmus cortices (non-hubs).

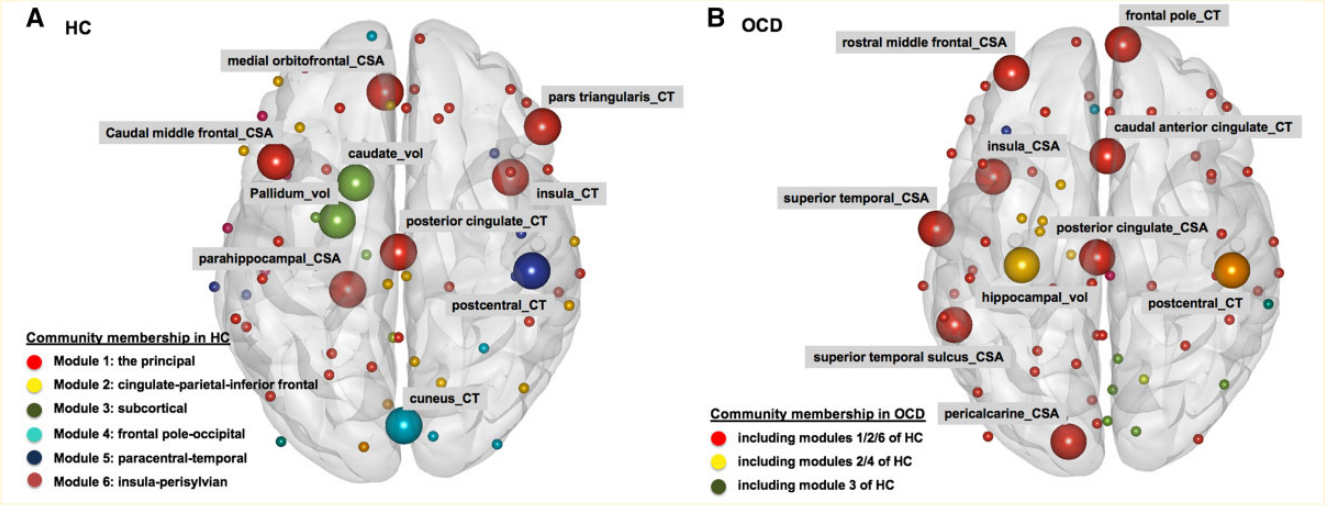

Figure 4 Meta-analysis of community membership and hubs. (**A**) Healthy bontrols (HC); and (**B**) OCD. Spheres represent nodes [= bi-laterally-averaged values of 33 cortical surface areas (CSAs), 33 cortical thickness (CT), and six subcortical volumes (vol)] comprising the intra-individual structural covariance network. Larger spheres represent hubs, and differential colours were used to denote the spheres (or network nodes) segregated as different modules.

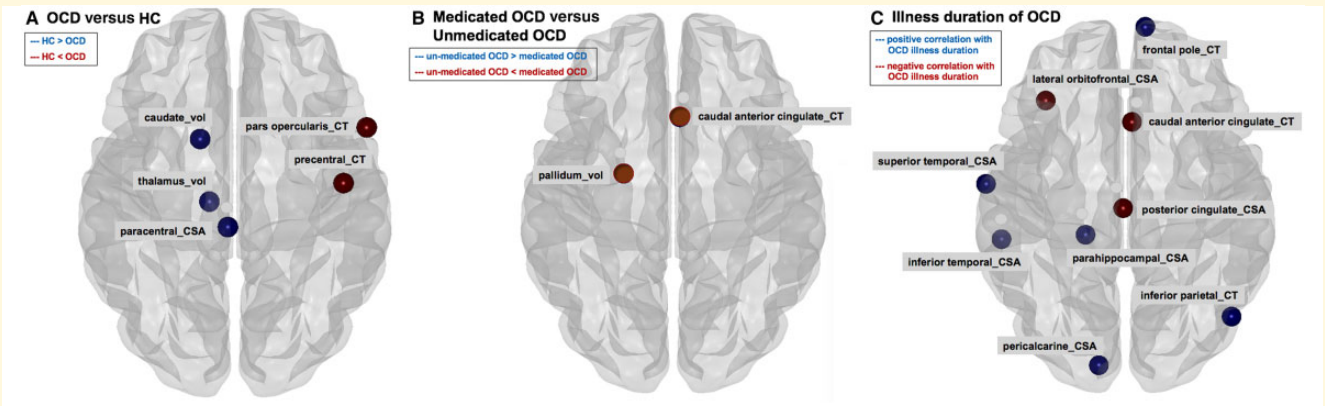

Figure 5 Meta-analysis of regional network characteristics (= rank-transformed betweenness, closeness, and eigenvector centralities). (**A**) Comparing OCD and healthy controls (HC); (**B**) comparing medicated OCD with unmedicated OCD; and (**C**) estimating the degrees of relationship with illness duration for OCD. CSA = cortical surface areas; CT = cortical thickness.

Discussion

The current meta-analysis of 37 datasets from 26 sites worldwide is the largest investigation of structural covariance networks in OCD to date. Two main findings emerged. First, we observed lower clustering, modularity, and small-worldness of OCD brain structural covariance networks compared with healthy controls, with community membership analysis confirming a less segregated organization of the global structural covariance network of OCD patients. Second, hub profiling demonstrated reduced centralities in subcortical volumes of caudate nucleus and thalamus as well as cortical surface area of paracentral cortex in OCD. Alterations in hub organization were associated with both medication status and illness duration. These novel findings are important; the first suggests a possible signature of altered brain morphometry in OCD compared to healthy controls, and the second provides evidence for OCD-related alterations in trajectories of brain development and maturation.

Lower clustering, modularity and small-worldness, but normal global efficiency, are indicative of lower global segregation, but spared global integration of OCD networks. In particular, lower modularity might be related to over-connectedness of certain nodes and diminished ability of the network to adapt flexibly (Guye *et al.*, 2010). This finding is consistent with previous observations of abnormal brain network segregation in functional networks in OCD (Zhang *et al.*, 2011). Small-worldness relates to an optimal network organization

that combines regional specialization and efficient global (Watts and Strogatz, 1998; Latora and Marchiori, 2001; Lefort-Besnard *et al.*, 2018). Thus, despite intact global efficiency, decreased levels of small-worldness and modularity in OCD point to a disrupted hierarchical network architecture.

Global network findings were not impacted by medication status or illness duration. This contrasts with previous research, which although based on functional MRI data, suggested that abnormal global network characteristics may depend on psychotropic treatment (Shin *et al.*, 2014). Although it is theoretically possible that the effects of psychotropic medication on OCD brain morphology differ in the acute versus chronic stage of pharmacotherapy so that there the net result over time is one of no change, there is little evidence to support this idea. In our view, a more plausible conclusion is that the lower global network segregation found here may represent a possible signature of altered brain morphometry in OCD. Further research is needed to confirm this.

The study also found reduced centralities of caudate nucleus and thalamic volumes in OCD compared to healthy controls. This is in line with our previous multicentre megaanalysis, which showed increased thalamic volume in OCD compared to healthy controls, even though only in the paediatric patients (Boedhoe *et al.*, 2017). Likewise, caudate nucleus and thalamus showed marked expansion in OCD and in their unaffected siblings compared to healthy controls, suggesting genetic contributions to altered brain morphology (Shaw *et al.*, 2015). Of note, meta-analytic integration of task-related functional MRI studies demonstrated OCD-specific differences in functional activation of the caudate nucleus. Similarly, nodal efficiency of the caudate nucleus was reduced in OCD in a white matter-based structural connectivity network (Zhong *et al.*, 2014), in line with a resting state functional connectivity profile that showed increased intra-subcortical modular connections for caudate nucleus and thalamus in OCD (Vaghi *et al.*, 2017).

Our data emphasize that alterations in hubs in OCD are associated with illness duration. This is consistent with previous work suggesting brain-related changes during the development of OCD (van den Heuvel *et al.*, 2016). In particular, we found that centralities of brain regions including the cortical thickness of caudal anterior cingulate as well as the cortical surface areas for posterior cingulate and lateral orbitofrontal cortices, were associated with longer illness duration in OCD. As an interface between sensorimotor, limbic and executive networks, the caudal anterior cingulate plays a major role in attentional control (Margulies *et al.*, 2007) and self-referential sensorimotor processing (Jung *et al.*, 2015; Mao *et al.*, 2017), the posterior cingulate cortex and connected default mode network supports internally-directed cognition, participates in the control of arousal state, and interacts with other brain regions for attentional modulation and conscious awareness (Leech and Sharp, 2014). Orbitofrontal regions have also previously been emphasized in OCD. The hub findings reported here point to OCD-related alterations in trajectories of brain development and maturation, particularly in cingulate and orbitofrontal regions. However, these hypotheses will require confirmation in longitudinal studies.

This study has some limitations that deserve emphasis. First, the current study analysed datasets that were extracted from brain MRI data collected from 26 international research institutions using diverse acquisition parameters (Boedhoe *et al.*, 2017, 2018), which may have introduced systematic biases. Nevertheless, our meta-analytical approach took into account differential site effects. Second, although all brain segmentation results underwent quality check procedures prior to extraction of numerical values, we were unable to implement motion correction of structural images, and it is theoretically possible that estimates of group differences are inflated by uncorrected motion. Nevertheless, there is no reason to suspect increased motion in either group. Third, in the calculation of intra-individual structural covariance networks, the current study applied the bilaterally-averaged values of 33 cortical surface area regions of interest, 33 cortical thickness regions of interest, and six subcortical volume regions of interest and therefore did not explore the homologous connectivity between the brain regions. However, we would like to emphasize that patterns of brain cortical-subcortical morphological asymmetry in adult OCD are not significantly different from healthy controls (Kong *et al.*, 2019). Fourth, the current study did not explore the possible effect of other clinical features such as the severity of depressive or anxiety symptoms, and IQ score, on the brain morphological features, because of the lack of sufficient information. Fifth, this was a cross-sectional study and any conclusions regarding developmental trajectories are necessarily tentative.

Taken together, this study showed that the structural covariance networks of individuals with OCD are less segregated and show a reorganization of brain hubs, compared to healthy controls. These findings support the hypothesis that OCD brain abnormalities are best described at the network level and involve alterations in the hierarchical structure of the brain. The segregation findings here are important insofar as they suggest a possible signature of altered brain morphometry OCD, while the hub findings are useful in emphasizing the importance of OCD-related alterations in trajectories of brain development and maturation, particularly in cingulate and orbitofrontal regions.

Funding

This research was funded by Basic Science Research Program through the National Research Foundation of Korea (NRF) funded by the Ministry of Education (NRF-2017R1D1A1B03028464) and the Basic Research Laboratory Program through the National Research Foundation of Korea (NRF) (Grant no. 2018R1A4A1025891).

ENIGMA is supported, in part, by an NIH grant (U54 EB020403) for big data analytics.

Competing interests

P.D.A (Alberta Innovates Translational Health Chair in Child and Youth Mental Health). D.P.H. is now an employee of Genentech, Inc. working on projects unrelated to this publication. D.M-C. receives royalties for contributing articles to UpToDate, Wolters Kluwer Health and fees from Elsevier for editorial tasks (all unrelated to the submitted work). H.B.S. (Biohaven research support for clinical trial; Royalties from UpToDate, Inc and Cambridge University Press). N.S. (Lundbeck-IIT). P.M.T. has received a research grant from Biogen, Inc. unrelated to the topic of this paper. No further conflict of interest is reported.

Supplementary material

Supplementary material is available at *Brain* online.

Appendix 1

ENIGMA-OCD working group members

Odile3 A. van den Heuvel, Dan J. Stein, Premika S.W. Boedhoe, Paul M. Thompson, Neda Jahanshad, Chris Vriend, Yoshinari Abe, Stephanie H. Ameis, Alan Anticevic, Paul D. Arnold, Marcelo C. Batistuzzo, Francesco Benedetti, Jan C. Beucke, Irene Bollettini, Anushree Bose, Silvia Brem, Anna Calvo, Yuqi Cheng, Kang Ik K. Cho, Valentina Ciullo, Sara Dallaspezia, Damiaan Denys, Jamie D. Feusner, Jean-Paul Fouche, Mònica Giménez, Patricia Gruner, Derrek P. Hibar, Marcelo Q. Hoexter, Hao Hu, Chaim Huyser, Keisuke Ikari, Norbert Kathmann, Christian Kaufmann, Kathrin Koch, Jun Soo Kwon, Luisa Lazaro, Christine Lochner, Paulo Marques, Rachel Marsh, Ignacio Martínez-Zalacaín, David Mataix-Cols, José M. Menchón, Luciano Minuzzi, Pedro Morgado, Pedro Moreira, Takashi Nakamae, Tomohiro Nakao, Janardhanan C. Narayanaswamy, Erika L. Nurmi, Joseph O'Neill, John Piacentini, Fabrizio Piras, Federica Piras, Y.C. Janardhan Reddy, Joao R. Sato, H. Blair Simpson, Noam Soreni, Carles Soriano-Mas, Gianfranco Spalletta, Michael C. Stevens, Philip R. Szeszko, David F. Tolin, Ganesan Venkatasubramanian, Susanne Walitza, Zhen Wang, Guido A. van Wingen, Jian Xu, Xiufeng Xu, Je-Yeon Yun, Qing Zhao.

References

Aboud KS, Huo Y, Kang H, Ealey A, Resnick SM, Landman BA, et al. Structural covariance across the lifespan: brain development and aging through the lens of inter-network relationships. Hum Brain Mapp 2019; 40: 125–36.

Alexander-Bloch A, Raznahan A, Bullmore E, Giedd J. The convergence of maturational change and structural covariance in human cortical networks. J Neurosci 2013; 33: 2889–99.

Amlien IK, Fjell AM, Tamnes CK, Grydeland H, Krogsrud SK, Chaplin TA, et al. Organizing principles of human cortical development–thickness and area from 4 to 30 years: insights from comparative primate neuroanatomy. Cereb Cortex 2016; 26: 257–67.

Anticevic A, Hu S, Zhang S, Savic A, Billingslea E, Wasylink S, et al. Global resting-state functional magnetic resonance imaging analysis identifies frontal cortex, striatal, and cerebellar dysconnectivity in obsessive-compulsive disorder. Biol Psychiatry 2014; 75: 595–605.

Armstrong CC, Moody TD, Feusner JD, McCracken JT, Chang S, Levitt JG, et al. Graph-theoretical analysis of resting-state fMRI in pediatric obsessive-compulsive disorder. J Affect Disord 2016; 193: 175–84.

Boedhoe PSW, Schmaal L, Abe Y, Alonso P, Ameis SH, Anticevic A, et al. Cortical abnormalities associated with pediatric and adult obsessive-compulsive disorder: findings from the ENIGMA obsessive-compulsive disorder working group. Am J Psychiatry 2018; 175: 453–62.

Boedhoe PS, Schmaal L, Abe Y, Ameis SH, Arnold PD, Batistuzzo MC, et al. Distinct subcortical volume alterations in pediatric and adult OCD: a worldwide meta- and mega-analysis. Am J Psychiatry 2017; 174: 60–9.

Cao M, Huang H, Peng Y, Dong Q, He Y. Toward developmental connectomics of the human brain. Front Neuroanat 2016; 10: 25.

Das T, Borgwardt S, Hauke DJ, Harrisberger F, Lang UE, Riecher-Rossler A, et al. Disorganized gyrification network properties during the transition to psychosis. JAMA Psychiatry 2018; 75: 613–22.

de Vries FE, de Wit SJ, van den Heuvel OA, Veltman DJ, Cath DC, van Balkom A, et al. Cognitive control networks in OCD: a resting-state connectivity study in unmedicated patients with obsessive-compulsive disorder and their unaffected relatives. World J Biol Psychiatry 2017; 20: 230–42.

de Wit SJ, Alonso P, Schweren L, Mataix-Cols D, Lochner C, Menchon JM, et al. Multicenter voxel-based morphometry mega-analysis of structural brain scans in obsessive-compulsive disorder. Am J Psychiatry 2014; 171: 340–9.

Desikan RS, Segonne F, Fischl B, Quinn BT, Dickerson BC, Blacker D, et al. An automated labeling system for subdividing the human cerebral cortex on MRI scans into gyral based regions of interest. Neuroimage 2006; 31: 968–80.

Dice LR. Measures of the amount of ecologic association between species. Ecology 1945; 26: 297–302.

Draganski B, Gaser C, Busch V, Schuierer G, Bogdahn U, May A. Neuroplasticity: changes in grey matter induced by training. Nature 2004; 427: 311–2.

Dwyer DB, Harrison BJ, Yucel M, Whittle S, Zalesky A, Pantelis C, et al. Large-scale brain network dynamics supporting adolescent cognitive control. J Neurosci 2014; 34: 14096–107.

Eickhoff SB, Laird AR, Fox PM, Lancaster JL, Fox PT. Implementation errors in the GingerALE Software: description and recommendations. Hum Brain Mapp 2017; 38: 7–11.

Ferrer I, Blanco R, Carulla M, Condom M, Alcantara S, Olive M, et al. Transforming growth factor-alpha immunoreactivity in the developing and adult brain. Neuroscience 1995; 66: 189–99.

First MB, Spitzer RL, Gibbon M, Williams JBW. Structured clinical interview for DSM-IV-TR axis I disorders (SCID-I). New York, NY: New York State Psychiatric Institute, Biometrics Department; 2002.

Fischl B. FreeSurfer. Neuroimage 2012; 62: 774–81.

Fornito A, Zalesky A, Bullmore ET. Fundamentals of brain network analysis. London: Elsevier; 2016.

Fortunato S. Community detection in graphs. Phys Rep 2010; 486: 75–174.

Fouche JP, Du Plessis S, Hattingh C, Roos A, Lochner C, Soriano-Mas C, et al. Cortical thickness in obsessive-compulsive disorder: multisite mega-analysis of 780 brain scans from six centres. Br J Psychiatry 2017; 210: 67–74.

Gottlich M, Kramer UM, Kordon A, Hohagen F, Zurowski B. Decreased limbic and increased fronto-parietal connectivity in unmedicated patients with obsessive-compulsive disorder. Hum Brain Mapp 2014; 35: 5617–32.

Grisham JR, Brown TA, Campbell LA. The anxiety disorders interview schedule for DSM-IV (ADIS-IV). Comprehensive handbook of psychological assessment, vol 2: personality assessment. Hoboken, NJ: John Wiley & Sons Inc; 2004. p. 163–77.

Gürsel DA, Avram M, Sorg C, Brandl F, Koch K. Frontoparietal areas link impairments of large-scale intrinsic brain networks with aberrant fronto-striatal interactions in OCD: a meta-analysis of resting-state functional connectivity. Neurosci Biobehav Rev 2018; 87: 151–60.

Guye M, Bettus G, Bartolomei F, Cozzone PJ. Graph theoretical analysis of structural and functional connectivity MRI in normal and pathological brain networks. MAGMA 2010; 23: 409–21.

Hedges LV, Vevea JL. Fixed- and random-effects models in meta-analysis. Psychol Methods 1998; 3: 486–504.

Higgins JP, Thompson SG, Deeks JJ, Altman DG. Measuring inconsistency in meta-analyses. BMJ 2003; 327: 557–60.

Hoagey DA, Rieck JR, Rodrigue KM, Kennedy KM. Joint contributions of cortical morphometry and white matter microstructure in healthy brain aging: a partial least squares correlation analysis. Hum Brain Mapp 2019; 40: 5315–29.

Hunt BA, Tewarie PK, Mougin OE, Geades N, Jones DK, Singh KD, et al. Relationships between cortical myeloarchitecture and electrophysiological networks. Proc Natl Acad Sci USA 2016; 113: 13510–5.

Jung WM, Lee IS, Wallraven C, Ryu YH, Park HJ, Chae Y. Cortical activation patterns of bodily attention triggered by acupuncture stimulation. Sci Rep 2015; 5: 12455.

Jung WH, Yucel M, Yun JY, Yoon YB, Cho KI, Parkes L, et al. Altered functional network architecture in orbitofronto-striato-thalamic circuit of unmedicated patients with obsessive-compulsive disorder. Hum Brain Mapp 2017; 38: 109–19.

Kaczkurkin AN, Park SS, Sotiras A, Moore TM, Calkins ME, Cieslak M, et al. Evidence for dissociable linkage of dimensions of psychopathology to brain structure in youths. Am J Psychiatry 2019; 176: 1000–9.

Kambeitz J, Kambeitz-Ilankovic L, Cabral C, Dwyer DB, Calhoun VD, van den Heuvel MP, et al. Aberrant functional whole-brain network architecture in patients with schizophrenia: a meta-analysis. Schizophr Bull 2016; 42: S13–21.

Kaufman J, Schweder AE. The schedule for affective disorders and schizophrenia for school age children: present and lifetime version (K-SADS-PL). In: M Hersen, DM Segal, M Hilsenroth, editors. The comprehensive handbook of psychological assessment (CHOPA), volume 2: personality assessment. New York: John Wiley and Sons; 2003.

Kawamoto T, Rosvall M. Estimating the resolution limit of the map equation in community detection. Phys Rev E Stat Nonlin Soft Matter Phys 2015; 91: 012809.

Kong XZ, Boedhoe PSW, Abe Y, Alonso P, Ameis SH, Arnold PD, et al. Mapping cortical and subcortical asymmetry in obsessive-compulsive disorder: findings from the ENIGMA Consortium. Biol Psychiatry 2019; pii: S0006-3223(19)31292-2.

Kremen WS, Fennema-Notestine C, Eyler LT, Panizzon MS, Chen CH, Franz CE, et al. Genetics of brain structure: contributions from the Vietnam era twin study of aging. Am J Med Genet B Genet 2013; 162: b751–61.

Krongold M, Cooper C, Bray S. Modular development of cortical gray matter across childhood and adolescence. Cereb Cortex 2017; 27: 1125–36.

Lancichinetti A, Fortunato S. Community detection algorithms: a comparative analysis. Phys Rev E 2009; 80: 056117.

Latora V, Marchiori M. Efficient behavior of small-world networks. Phys Rev Lett 2001; 87: 198701.

Leech R, Sharp DJ. The role of the posterior cingulate cortex in cognition and disease. Brain 2014; 137 (Pt 1): 12–32.

Lefort-Besnard J, Bassett DS, Smallwood J, Margulies DS, Derntl B, Gruber O, et al. Different shades of default mode disturbance in schizophrenia: subnodal covariance estimation in structure and function. Hum Brain Mapp 2018; 39: 644–61.

Makowski C, Lewis JD, Lepage C, Malla AK, Joober R, Lepage M, et al. Structural associations of cortical contrast and thickness in first episode psychosis. Cerebral Cortex 2019; 29: 5009–21.

Mao CV, Araujo MF, Nishimaru H, Matsumoto J, Tran AH, Hori E, et al. Pregenual anterior cingulate gyrus involvement in spontaneous social interactions in primates-evidence from behavioral, pharmacological, neuropsychiatric, and neurophysiological findings. Front Neurosci 2017; 11: 34.

Margulies DS, Kelly AM, Uddin LQ, Biswal BB, Castellanos FX, Milham MP. Mapping the functional connectivity of anterior cingulate cortex. Neuroimage 2007; 37: 579–88.

Mechelli A, Friston KJ, Frackowiak RS, Price CJ. Structural covariance in the human cortex. J Neurosci 2005; 25: 8303–10.

Menzies L, Chamberlain SR, Laird AR, Thelen SM, Sahakian BJ, Bullmore ET. Integrating evidence from neuroimaging and neuropsychological studies of obsessive-compulsive disorder: the orbitofronto-striatal model revisited. Neurosci Biobehav Rev 2008; 32: 525–49.

Milad MR, Rauch SL. Obsessive-compulsive disorder: beyond segregated cortico-striatal pathways. Trends Cogn Sci 2012; 16: 43–51.

Newman ME. Modularity and community structure in networks. Proc Natl Acad Sci USA 2006; 103: 8577–82.

Palaniyappan L, Marques TR, Taylor H, Mondelli V, Reinders A, Bonaccorso S, et al. Globally efficient brain organization and treatment response in psychosis: a connectomic study of gyrification. Schizophr Bull 2016; 42: 1446–56.

Piras F, Piras F, Chiapponi C, Girardi P, Caltagirone C, Spalletta G. Widespread structural brain changes in OCD: a systematic review of voxel-based morphometry studies. Cortex 2015; 62: 89–108.

Posner J, Marsh R, Maia TV, Peterson BS, Gruber A, Simpson HB. Reduced functional connectivity within the limbic cortico-striato-thalamo-cortical loop in unmedicated adults with obsessive-compulsive disorder. Hum Brain Mapp 2014; 35: 2852–60.

Power JD, Cohen AL, Nelson SM, Wig GS, Barnes KA, Church JA, et al. Functional network organization of the human brain. Neuron 2011; 72: 665–78.

Power JD, Schlaggar BL, Lessov-Schlaggar CN, Petersen SE. Evidence for hubs in human functional brain networks. Neuron 2013; 79: 798–813.

Pujol J, Soriano-Mas C, Alonso P, Cardoner N, Menchon JM, Deus J, et al. Mapping structural brain alterations in obsessive-compulsive disorder. Arch Gen Psychiatry 2004; 61: 720–30.

Qi T, Schaadt G, Cafiero R, Brauer J, Skeide MA, Friederici AD. The emergence of long-range language network structural covariance and language abilities. Neuroimage 2019; 191: 36–48.

Raudenbush SW. Analyzing effect sizes: random effects models. New York: Russell Sage Foundation; 2009.

Reess TJ, Rus OG, Gursel DA, Schmitz-Koep B, Wagner G, Berberich G, et al. Network-based decoupling of local gyrification in obsessive-compulsive disorder. Hum Brain Mapp 2018a; 39: 3216–26.

Reess TJ, Rus OG, Gürsel DA, Schmitz-Koep B, Wagner G, Berberich G, et al. Network-based decoupling of local gyrification in obsessive-compulsive disorder. Hum Brain Mapp 2018b; 39: 3216–26.

Reess TJ, Rus OG, Schmidt R, de Reus MA, Zaudig M, Wagner G, et al. Connectomics-based structural network alterations in obsessive-compulsive disorder. Transl Psychiatry 2016; 6: e882.

Reichardt J, Bornholdt S. Statistical mechanics of community detection. Phys Rev E Stat Nonlin Soft Matter Phys 2006; 74 (Pt 2): 016110.

Richmond S, Johnson KA, Seal ML, Allen NB, Whittle S. Development of brain networks and relevance of environmental and genetic factors: a systematic review. Neurosci Biobehav Rev 2016; 71: 215–39.

Rosvall M, Bergstrom CT. An information-theoretic framework for resolving community structure in complex networks. Proc Natl Acad Sci USA 2007; 104: 7327–31.

Rubinov M, Sporns O. Complex network measures of brain connectivity: uses and interpretations. Neuroimage 2010; 52: 1059–69.

Schmaal L, Yucel M, Ellis R, Vijayakumar N, Simmons JG, Allen NB, et al. Brain structural signatures of adolescent depressive symptom trajectories: a longitudinal magnetic resonance imaging study. J Am Acad Child Adolesc Psychiatry 2017; 56: 593–601.e9.

Schmidt FL, Oh IS, Hayes TL. Fixed- versus random-effects models in meta-analysis: model properties and an empirical comparison of differences in results. Br J Math Stat Psychol 2009; 62 (Pt 1): 97–128.

Seidlitz J, Vasa F, Shinn M, Romero-Garcia R, Whitaker KJ, Vertes PE, et al. Morphometric similarity networks detect microscale cortical organization and predict inter-individual cognitive variation. Neuron 2018a; 97: 231–47.e7.

Seidlitz J, Váša F, Shinn M, Romero-Garcia R, Whitaker KJ, Vértes PE, et al. Morphometric similarity networks detect microscale cortical organization and predict inter-individual cognitive variation. Neuron 2018b; 97: 231–47.e7.

Sharda M, Foster NEV, Tryfon A, Doyle-Thomas KAR, Ouimet T, Anagnostou E, et al. Language ability predicts cortical structure and covariance in boys with autism spectrum disorder. Cereb Cortex 2017; 27: 1849–62.

Shaw P, Sharp W, Sudre G, Wharton A, Greenstein D, Raznahan A, et al. Subcortical and cortical morphological anomalies as an endophenotype in obsessive-compulsive disorder. Mol Psychiatry 2015; 20: 224–31.

Sheehan DV, Lecrubier Y, Sheehan KH, Amorim P, Janavs J, Weiller E, et al. The Mini-International Neuropsychiatric Interview (M.I.N.I.): the development and validation of a structured diagnostic psychiatric interview for DSM-IV and ICD-10. J Clin Psychiatry 1998; 59: 22–33; quiz 4-57.

Shin DJ, Jung WH, He Y, Wang J, Shim G, Byun MS, et al. The effects of pharmacological treatment on functional brain connectome in obsessive-compulsive disorder. Biol Psychiatry 2014; 75: 606–14.

Silverman WK, Saavedra LM, Pina AA. Test-retest reliability of anxiety symptoms and diagnoses with the Anxiety Disorders Interview Schedule for DSM-IV: child and parent versions. J Am Acad Child Adolesc Psychiatry 2001; 40: 937–44.

Solé-Casals J, Serra-Grabulosa JM, Romero-Garcia R, Vilaseca G, Adan A, Vilaro N, et al. Structural brain network of gifted children has a more integrated and versatile topology. Brain Struct Funct 2019; 224: 2373–83.

Soriano-Mas C, Harrison BJ. Brain functional connectivity in Obsessive-Compulsive disorder. Oxford: Oxford University Press; 2017.

Soriano-Mas C, Harrison BJ, Pujol J, Lopez-Sola M, Hernandez-Ribas R, Alonso P, et al. Structural covariance of the neostriatum with regional gray matter volumes. Brain Struct Funct 2013; 218: 697–709.

Spreng RN, DuPre E, Ji JL, Yang G, Diehl C, Murray JD, et al. Structural covariance reveals alterations in control and salience network integrity in chronic schizophrenia. Cereb Cortex 2019; 29: 5269–84.

Subira M, Cano M, de Wit SJ, Alonso P, Cardoner N, Hoexter MQ, et al. Structural covariance of neostriatal and limbic regions in patients with obsessive-compulsive disorder. J Psychiatry Neurosci 2016; 41: 115–23.

Sussman D, Leung RC, Chakravarty MM, Lerch JP, Taylor MJ. The developing human brain: age-related changes in cortical, subcortical, and cerebellar anatomy. Brain Behav 2016; 6: e00457.

Takagi Y, Sakai Y, Lisi G, Yahata N, Abe Y, Nishida S, et al. A neural marker of obsessive-compulsive disorder from whole-brain functional connectivity. Sci Rep 2017; 7: 7538.

Uehara T, Yamasaki T, Okamoto T, Koike T, Kan S, Miyauchi S, et al. Efficiency of a "small-world" brain network depends on consciousness level: a resting-state FMRI study. Cereb Cortex 2014; 24: 1529–39.

Vaghi MM, Vertes PE, Kitzbichler MG, Apergis-Schoute AM, van der Flier FE, Fineberg NA, et al. Specific frontostriatal circuits for impaired cognitive flexibility and goal-directed planning in obsessive-compulsive disorder: evidence from resting-state functional connectivity. Biol Psychiatry 2017; 81: 708–17.

van den Heuvel OA, van Wingen G, Soriano-Mas C, Alonso P, Chamberlain SR, Nakamae T, et al. Brain circuitry of compulsivity. Eur Neuropsychopharmacol 2016; 26: 810–27.

Viechtbauer W. Conducting meta-analyses in R with the metafor Package. J Stat Soft 2010; 36: 1–48.

Vijayakumar N, Allen NB, Youssef G, Dennison M, Yucel M, Simmons JG, et al. Brain development during adolescence: a mixed-longitudinal investigation of cortical thickness, surface area, and volume. Hum Brain Mapp 2016; 37: 2027–38.

Vriend C, van den Heuvel OA, Berendse HW, van der Werf YD, Douw L. Global and subnetwork changes of the structural connectome in de novo Parkinson's disease. Neuroscience 2018; 386: 295–308.

Vuoksimaa E, Panizzon MS, Chen CH, Fiecas M, Eyler LT, Fennema-Notestine C, et al. Is bigger always better? The importance of cortical configuration with respect to cognitive ability. Neuroimage 2016; 129: 356–66.

Wannan CMJ, Cropley VL, Chakravarty MM, Bousman C, Ganella EP, Bruggemann JM, et al. Evidence for network-based cortical thickness reductions in schizophrenia. Am J Psychiatry 2019; 176: 552–63.

Watts DJ, Strogatz SH. Collective dynamics of 'small-world' networks. Nature 1998; 393: 440–2.

Wee CY, Yap PT, Shen D. Prediction of Alzheimer's disease and mild cognitive impairment using cortical morphological patterns. Hum Brain Mapp 2013; 34: 3411–25.

Weinberg D, Lenroot R, Jacomb I, Allen K, Bruggemann J, Wells R, et al. Cognitive subtypes of schizophrenia characterized by differential brain volumetric reductions and cognitive decline. JAMA Psychiatry 2016; 73: 1251–9.

Yun JY, Jang JH, Kim SN, Jung WH, Kwon JS. Neural correlates of response to pharmacotherapy in obsessive-compulsive disorder: individualized cortical morphology-based structural covariance. Prog Neuropsychopharmacol Biol Psychiatry 2015; 63: 126–33.

Yun JY, Kim SN, Lee TY, Chon MW, Kwon JS. Individualized covariance profile of cortical morphology for auditory hallucinations in first-episode psychosis. Hum Brain Mapp 2016; 37: 1051–65.

Zaremba D, Dohm K, Redlich R, Grotegerd D, Strojny R, Meinert S, et al. Association of brain cortical changes with relapse in patients with major depressive disorder. JAMA Psychiatry 2018; 75: 484–92.

Zhang T, Wang J, Yang Y, Wu Q, Li B, Chen L, et al. Abnormal small-world architecture of top-down control networks in obsessive-compulsive disorder. J Psychiatry Neurosci 2011; 36: 23–31.

Zhong Z, Zhao T, Luo J, Guo Z, Guo M, Li P, et al. Abnormal topological organization in white matter structural networks revealed by diffusion tensor tractography in unmedicated patients with obsessive-compulsive disorder. Prog Neuropsychopharmacol Biol Psychiatry 2014; 51: 39–50.

Zielinski BA, Gennatas ED, Zhou J, Seeley WW. Network-level structural covariance in the developing brain. Proc Natl Acad Sci USA 2010; 107: 18191–6.